Malaysian Journal of Mathematical Sciences 20(2): 659–682 (2026)
https://doi.org/10.47836/mjms.20.2.11

Malaysian Journal of Mathematical Sciences

Journal homepage: https://mjms.upm.edu.my

Analysis of Hepatitis C Virus Dynamics with Dual Transmissions using Sliding Mode Controller

Pichani, C.[1] and Chinnathambi, R.*[1]

[1]*Department of Mathematics, School of Advanced Sciences, Vellore Institute of Technology, Chennai, Tamilnadu-600 127, India*

E-mail: rajivganthi.c@vit.ac.in
**Corresponding author*

Received: 1 March 2025
Accepted: 31 October 2025

Abstract

This work describes a HCV model infection with four state variables, such as uninfected and infected hepatocytes, antibodies, virions. Here, the model contains dual transmission rate such that the disease can be transmitted by infected cell also. The model incorporates two control inputs: ribavirin, which suppresses virion generation, and pegylated interferon(peg-IFN-α), which targets infected hepatocytes. Four novel non-linear control schemes are introduced, which as the integer and fractional-order terminal, integral, double integral sliding mode controller. These controllers attempt to maximize the uninfected hepatocytes, antibodies and minimize the virions, infected hepatocytes to zero. We studied the comparison results of these controllers. Numerical simulations validate the theoretical conclusions.

Keywords: HCV model; Lyapunov function; sliding mode controller; stability.

1 Introduction

Hepatitis C Virus (HCV) is a blood-borne infection primarily impacting the liver, resulting in inflammation and potentially severe long-term consequences. HCV represents an important public health challenge globally related to its extensive prevalence and elevated risk of chronic infection. The virus is predominantly transmitted via blood-to-blood contact, which can occur through various types such as unscreened blood transfusions, organ transplants from infected donors, needle sharing among intravenous drug users, and the use of inadequately sterilized medical or tattooing instruments. Moreover, HCV can be transmitted vertically from an infected mother to her infant during childbirth and during sexual intercourse with an infected partner [27]. Chronic liver infection affects almost 85% of HCV cases, resulting in complications in other organs. Symptoms involve common fatigue, nausea, abdominal pain, dark urine, and jaundice. To prevent HCV infection, avoid using drug paraphernalia, guarantee blood donors undergo testing, engage in safe sexual practices, and utilize adequately sterilized medical and tattooing instruments.

In 2023, the World Health Organization (WHO) estimated that approximately 58 million people worldwide are living with chronic HCV infection, with 3.2 million of those cases occurring in children and adolescents. Currently there is no vaccine available for HCV. However, several treatments are available, including pegylated-interferon-alpha$(IFN-\alpha)$, ribavirin, and Direct-Acting Antivirals (DAAs) [5]. Mathematical modelling facilitates the integration of all relevant factors, offering a significant insight into disease progression and the effects of treatment [30]. The authors in [19] investigates the dynamics of a soft tumor-immune system model influenced by random noise, analyzing how stochastic fluctuations impact tumor growth and immune response interactions. Fractional-order modeling effectively captures memory and hereditary effects in complex systems. Glycerol hydrogenolysis via heterogeneous catalysis modeled with fractional kinetics [31]. The authors in [3] used the sustainable fractal-fractional method to quantify disparities in atmospheric chemical modeling. Xu et al. [29] discussed the dynamical analysis of fractional SEI_rI_sR model. Maharajan et al. [9] derived exponential stability conditions for delay-dependent complex-valued BAM neural networks under stochastic and impulsive effects. Shukla et al. [22] proposed an adaptive fixed-time synchronization method ensuring rapid convergence in chaotic dynamical systems.

Neumann et al. [12] studied the basic mathematical models for HBV and HIV infections. Rihan et al. [18] discussed a stochastic delay differential model for HBV infection, focusing on solution existence, stationary distributions, and disease extinction conditions, and highlighting the effects of stochastic perturbations and time delays. The authors in [16] presented a fractional-order model for HCV infection, incorporating interferon-α treatment and a time delay for intracellular processes to enhance understanding of HCV dynamics. Woyes et al. [28] examined HCV transmission among people who inject drugs, highlighting the critical impact of injecting behavior and the importance of harm reduction strategies. Stocks et al. [24] investigated the HCV model among those who inject drugs to identify undiagnosed cases and evaluate the effects of interventions, thereby supporting the WHO's elimination objectives. The authors [17] studied a fractional-order model for HCV replication, accounting for interferon-α effects and intracellular delays.

Optimal control is an essential component of bio-mathematics, especially in the domains of epidemiology and ecology [2]. This approach entails identifying the most effective control strategies to optimize overall performance[8, 10]. Mandal et al. [11] proposed the model to study hepatocyte apoptosis and CTL response in chronic HCV infection, emphasizing its impact on liver damage and the effectiveness of DAAs in viral eradication. Hagger et al. [4] employs the perturbation iteration method to solve the HBV optimal control problem under treatment, yielding accurate

results consistent with other methods and effectively capturing drug response dynamics. Simon et al. [23] formulated an optimal control model for a predator prey system incorporating disease dynamics in the prey population to identify strategies that minimize infection and ecological imbalance.

Wang et al. [26] developed a model for HCV that includes DAAs, virus transmission modes, and immune response, emphasizing the need to monitor viral load for effective treatment using dual transmission dynamics. The authors in [25] explored the HCV infection dynamics using a multiscale model that includes virus-to-cell and cell-to-cell transmission, along with Cytotoxic T lymphocyte and antibody responses. Shi et al. [21] analyzed fractional-order systems with seismic and delay effects, proposing a novel switching surface and establishing stability via LMIs and Lyapunov-Krasovskii theory, validated through Sliding Mode Controller (SMC) based simulations. Rehman et al. [15] studied the HCV model, introducing controllers for antiviral therapy that preserve uninfected hepatocytes while targeting infected cells, comparing SMC with Integral super twisting SMC. Hamza et al. [6] discussed a nonlinear mathematical model for treating HCV that uses two control inputs to manage infected cells and reduce viral load, enhancing treatment outcomes by the comparison of different sliding mode controllers.

In this study, we develop a novel HCV infection model that incorporates dual transmission routes via both infected cells and free virions. Two antiviral controls are introduced: ribavirin, which inhibits viral production, and pegylated interferon(peg-IFN-α), which targets infected cells. The main highlights of this work is given as below:

- Describe a four advanced nonlinear controllers as integer and fractional-order terminal, integral, double integral sliding mode controller.
- Lyapunov-based analysis ensures stability and convergence results, for each control strategy.
- A comparative analysis of the performance for these controllers conducted.
- Demonstration through simulations that effective viral suppression and recovery can be achieved within a short-term clinical time frame(5 to 7 weeks).

These contributions provide a more accurate and control-responsive framework for HCV treatment analysis. This manuscript is organized as follows: Section 2 describes the formulation of the model with control inputs. Section 3 shows the dynamic control strategy of the model and also the comparison results. Numerical simulations that validate theoritical results are explained in Section 4. Section 5 gives the conclusion of the work.

2 Formulation of Mathematical Model

Hamza et al. [6] studied the dynamics of HCV model with the compartments of uninfected hepatocytes $T(t)$, infected hepatocytes $I(t)$ and virions $V(t)$,

$$\begin{aligned}
\frac{dT(t)}{dt} &= m + r_T T\left(1 - \frac{T+I}{T_{\max}}\right) - (1-u_1)\beta TV - d_T T,\\
\frac{dI(t)}{dt} &= (1-u_1)\beta TV + r_I I\left(1 - \frac{T+I}{T_{\max}}\right) - \delta I,\\
\frac{dV(t)}{dt} &= (1-u_2)pI - cV.
\end{aligned} \tag{1}$$

The rate of production and mortality of T are m and d_T, respectively. r_T denotes proliferation rate or the maximal per capita growth rate of T, whereas $T_{\max}$ represents the maximum capacity of uninfected hepatocytes, regulated within a logistic growth model. β is the rate of infection for HCV. r_I is maximal per capita growth rate or the proliferation rate of infected hepatocytes. The mortality rate of infected hepatocytes is δ. The elimination rate of the virus is c. The production of virions is assumed to be inhibited by interferon and ribavirin treatments, represented as control variables u_1 and u_2. p represents the rate at which the virus is produced. In the model (1), we include another transmission rate in which the disease is transmitted by the infected [20], so that we add control in the transmission of infected and uninfected cells. Recovery is incorporated into the infected hepatocyte population, along with an immune response compartment denoted by $W(t)$. Consequently, the model is formulated as:

$$\begin{aligned}
\frac{dT(t)}{dt} &= m + r_T T\left(1 - \frac{T+I}{T_{\max}}\right) - \beta_1 TV - (1-u_1)\beta_2 TI - d_T T + \rho I,\\
\frac{dI(t)}{dt} &= \beta_1 TV + (1-u_1)\beta_2 TI + r_I I\left(1 - \frac{T+I}{T_{\max}}\right) - \delta I - \rho I,\\
\frac{dV(t)}{dt} &= (1-u_2)pI - cV - qVW,\\
\frac{dW(t)}{dt} &= gVW - dW.
\end{aligned} \tag{2}$$

Here, β_2 represents the transmission rate from infected cell to uninfected cell. ρ is the recovery rate of infected cells. q represents the rate at which antibodies neutralize the viral load. g represents the rate of antibody development due to free virions, while d indicates the rate of immune response decay. The model is visually represented through a schematic diagram in Figure 1.

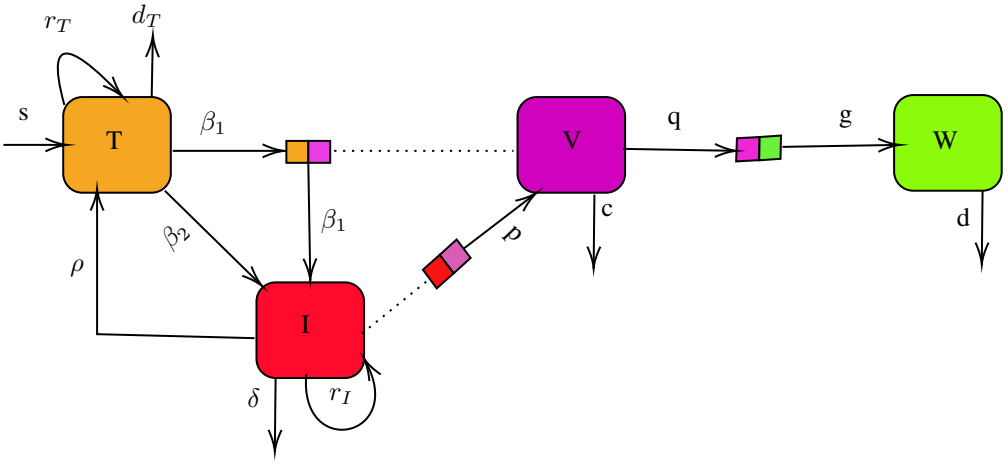

Figure 1: Schematic representation of the model.

To improve clarity, the variable notation has been changed from T, I, V, and W to x_1, x_2, x_3 and

x_4, respectively;

$$\begin{aligned}
\frac{dx_1(t)}{dt} &= m + r_T x_1 \left(1 - \frac{x_1 + x_2}{T_{\max}}\right) - \beta_1 x_1 x_3 - (1-u_1)\beta_2 x_1 x_2 - d_T x_1 + \rho x_2, \\
\frac{dx_2(t)}{dt} &= \beta_1 x_1 x_3 + (1-u_1)\beta_2 x_1 x_2 + r_I x_2 \left(1 - \frac{x_1 + x_2}{T_{\max}}\right) - \delta x_2 - \rho x_2, \\
\frac{dx_3(t)}{dt} &= (1-u_2) p x_2 - c x_3 - q x_3 x_4, \\
\frac{dx_4(t)}{dt} &= g x_3 x_4 - d x_4.
\end{aligned} \tag{3}$$

In the chronic HCV mathematical model, the variables u_1 and u_2 represent control inputs that quantify the effectiveness of therapeutic interventions, specifically ribavirin and pegylated interferon-alpha(peg-IFN-α) treatments. These interventions primarily aim to regulate the development of virions x_3 and dynamics of infected hepatocytes x_2 . The model shows that u_1 reduces the population of infected hepatocytes x_2 by $(1-u_1)$ and u_2 decreases virion production x_3 by a factor of $(1-u_2)$. It is crucial to emphasize that the control actions u_1 and u_2 in our suggested solution do not represent the dynamics of a direct drug-dependent device.

This specifically focuses on preserving uninfected hepatocytes while simultaneously decreasing the development of virions and the quantity of infected hepatocytes. Consequently, the inputs of these controls serve as theoretical frameworks for the intervention strategies instead of being direct applications of drug delivery systems.

2.1 Non-negativity and boundedness

Theorem 2.1. *Given the non-negative initial conditions $T(0)$, $I(0)$, $V(0)$ and $W(0)$, all solutions of the model (2) are non negative, for all $t \geq 0$.*

Proof. From the model (2), we have

$$\begin{aligned}
\frac{dT}{dt}|_{T=0} &= m + \rho I \geq 0, && \text{for all} \quad I \geq 0, \\
\frac{dI}{dt}|_{I=0} &= \beta_1 T I \geq 0, && \text{for all} \quad T \geq 0, \quad I \geq 0, \\
\frac{dV}{dt}|_{V=0} &= (1-u_2) p I \geq 0, && \text{for all} \quad I \geq 0, \\
\frac{dW}{dt}|_{W=0} &= 0 \geq 0.
\end{aligned}$$

Therefore, the solution of (2) is positive. □

Theorem 2.2. *Let $X(t)$ be the unique solution of (2) for any $t \geq 0$, then the solution $X(t)$ is bounded above, such that $X(t) \in \Omega$ where Ω is the feasible region.*

Proof. By adding the left and right equations of model(2), we obtain

$$\begin{aligned}\frac{dN}{dt} &= m + \left(1 - \frac{T+I}{T_{\max}}\right)(r_T T + r_I I) - (d_T T + \delta I + cV + dW) + (1-u_2)pI,\\ &\leq m + r_{\max} + pI - D_{\min} N, \qquad r_{\max} = \max(r_T, r_I), \qquad d_N = \min\{d_T, \delta, c, d\},\\ \frac{dN}{dt} &\leq m - CN, \qquad C = d_N - (r_{\max} + p).\end{aligned}$$

Solving the inequality, we obtain

$$N(t) \leq \left(N(0) - \frac{m}{C}\right) e^{-Ct} + \frac{m}{C}.$$

Consequently, Ω is positively invariant. However if $N(0) \geq \dfrac{m}{C}$, then either the solution enters the finite time or $N(t)$ approaches $\dfrac{m}{C}$ as $t \to \infty$. Therefore, every solution of model (2) in $\mathbb{R}^4_+$ is ultimately bounded within Ω. □

3 Dynamic Control Strategy

Numerous nonlinear control systems have been devised, with sliding mode control being particularly useful for variable structure systems. The nonlinear control approach offers high precision, minimal steady-state error, and strong robustness against external disturbances and model uncertainties. It is simple to implement and achieves convergence within a finite time, offering an advantage over other nonlinear control methods [7]. To reduce the Steady State Error (SSE) and chattering, higher order SMC has been considered.

In SMC, we initially establish $S = 0$ which is sliding surface in order to achieve the desired control objectives. We develop a control law that restricts the system's dynamics to this surface. The sliding coefficient controls the speed at which the system's trajectory approaches the sliding surface. Moreover, a chattering phenomena can occur in sliding mode control implementations. A robust reachability criterion is employed to formulate the control to minimize this chattering effect by the consideration of

$$\dot{S}_i = -K|S_i|^{\alpha} sign\left(\frac{S_i}{\phi_i}\right), \tag{4}$$

where α is a unit inside the interval 0 and 1. The term $|S_i|^{\alpha}$ enhances the control input S_i in such a way that the reaching speed increases when the state is far from the sliding surface, but decreases as it approaches the sliding surface. Additionally, the magnitude of chattering can be minimized by interpolating S_i within a thin boundary layer of thickness ϕ. ϕ_i is taken as a positive number which is smaller. K represents a sufficiently large positive gain and the Signum function, denoted as $sign$, is defined as follows,

$$Sign(S) = \begin{cases} -1 & \text{if} \quad S < 0,\\ 0 & \text{if} \quad S = 0,\\ 1 & \text{if} \quad S > 0. \end{cases} \tag{5}$$

In SMC, the control input is divided into two components,

$$u(t) = u_{nom} + u_{sw},$$

where, u_{nom} denotes the nominal Sliding mode control law that directs the system towards the equilibrium point, whereas u_{sw} signifies the switching SMC control law. This switching element guarantees that the system's trajectory that remains on the sliding surface until it attains the origin. The sliding surface has been defines as,

$$S = [S_1, S_2, \ldots, S_n]^T, \tag{6}$$

where $S_1, S_2, \ldots, S_n$ represent distinct sliding surfaces corresponding to different system outputs, each designed to achieve specific control objectives for the associated output variables as Figure 2.

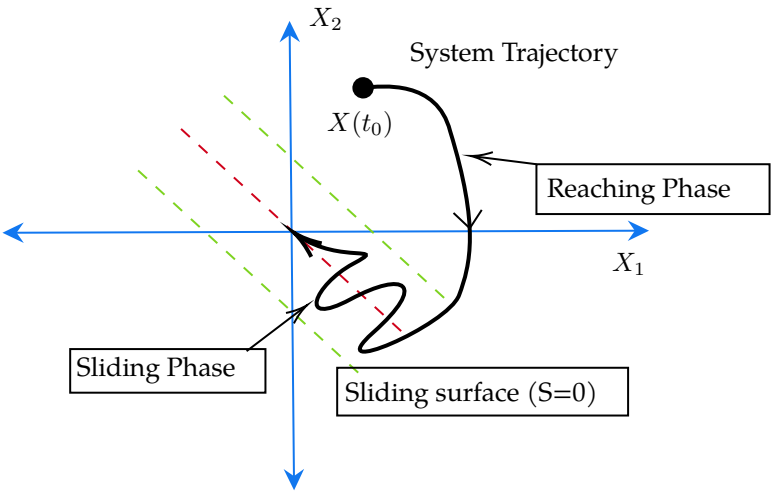

Figure 2: Phase plane representation of sliding mode control.

The following assumptions for the SMC are discussed below;

- The design coefficient k is a non-negative real number greater than zero.
- ϕ and α are the deisgn parameter that ranges between 0 and 1.
- The gains related to the sliding surfaces which are positive real values greater than zero.
- The considered Lyapunov function is always a positive definite.

This study proposes and analyzes four nonlinear sliding mode controllers to regulate HCV dynamics under dual transmission routes. Each controller reflects specific biological behaviors and treatment responses. The Integral Sliding Mode Controller(ISMC) ensures robustness from the start, representing steady treatment efforts compensating for immune or drug variability. The Terminal Sliding Mode Controller(TSMC) offers finite-time convergence, ideal for rapid suppression strategies. The Double Integral Sliding Mode Controller(DISMC) improves tracking accuracy and reduces chattering, aligning with smoother, cumulative treatment protocols. The Fractional-Order Terminal Sliding Mode Controller(FOTSMC) adds control flexibility by capturing memory effects like immune delay, better reflecting biological reality.

3.1 Integral sliding mode control

ISMC is an adaptation of sliding mode control that integrates integral action into the control structure. This augmentation improves robustness and diminishes steady-state error. ISMC integrates the benefits of classical SMC with integral feedback, making it especially efficient for systems subjected to uncertainties and disturbances. We then introduce error terms to establish a relationship between the states x_2 and x_3 and their respective reference values $x_{2_{ref}}$ and $x_{3_{ref}}$.

$$e_1 = x_2 - x_{2_{ref}}, \quad e_3 = x_3 - x_{3_{ref}}, \quad e_2 = \int e_1, \quad e_4 = \int e_3.$$

An error integral term was incorporated into the sliding surface "S_1" and "S_2" which represent for the infected hepatocytes and virions given as follows,

$$\begin{cases} S_1 = a_1 e_1 + a_2 e_2, \\ S_2 = a_3 e_3 + a_4 e_4. \end{cases} \tag{7}$$

The coefficients a_1, a_2, a_3 and a_4 govern the rate at which the system converges to the sliding surface, influencing its stability and performance. Taking derivative with respect to time for the sliding surfaces, substituting e_1 and e_2, and then substituting S_1 and S_2 from (3) enables us to derive the control input law for x_2 and x_3. By solving the system, we determine the control inputs required to effectively manage the compartments of infected cells and virions. In ISMC, two control laws, u_{nom} and u_{sw}, are

$$\begin{aligned} u_{nom} = \frac{1}{a_1\beta_2 x_1 x_2} \Bigg[& a_1\beta_1 x_1 x_3 + a_1\beta_2 x_1 x_2 + r_I a_1 x_2 \left(1 - \frac{x_1 + x_2}{T_{\max}}\right) \\ & - a_1\delta x_2 - a_1\rho x_2 - a_1 \dot{x_{2_{ref}}} + a_2 e_1 \Bigg], \\ u_{sw} = \frac{1}{a_1\beta_2 x_1 x_2} & \left[K_1 |S_1|^{\alpha} sign\left(\frac{S_1}{\phi_1}\right) \right]. \end{aligned} \tag{8}$$

By incorporating the switching and nominal Sliding mode control laws from (8) and resolving the control input u_1, we get

$$\begin{aligned} u_1(t) = \frac{1}{a_1\beta_2 x_1 x_2} \Bigg[& a_1\beta_1 x_1 x_3 + a_1\beta_2 x_1 x_2 + K_1 |S_1|^{\alpha} sign\left(\frac{S_1}{\phi_1}\right) \\ & + r_I a_1 x_2 \left(1 - \frac{x_1 + x_2}{T_{\max}}\right) - a_1\delta x_2 - a_1\rho x_2 - a_1 \dot{x_{2_{ref}}} + a_2 e_1 \Bigg]. \end{aligned} \tag{9}$$

Similarly, the sliding manifold can be described in terms of reducing virions by management of the input $u_2(t)$ as,

$$\begin{aligned} u_{nom} &= \frac{1}{a_3 p x_2} \left[a_3 p x_2 - a_3 c x_3 - a_3 q x_3 x_4 - a_3 \dot{x_{3ref}} + a_4 e_3 \right], \\ u_{sw} &= \frac{1}{a_3 p x_2} \left[K_2 |S_2|^{\alpha} sign\left(\frac{S_2}{\phi_2}\right) \right]. \end{aligned} \tag{10}$$

By combining we get,

$$u_2(t) = \frac{1}{a_3 p x_2} \left[a_3 p x_2 + K_2 |S_2|^{\alpha} sign\left(\frac{S_2}{\phi_2}\right) - a_3 c x_3 - a_3 q x_3 x_4 - a_3 \dot{x_{3ref}} + a_4 e_3 \right]. \tag{11}$$

The control input u_2, as described by (11), serves as the required control input to regulate the virion dynamics and ensure they track their reference value.

In order to demonstrate the stability of the proposed controller, the following Lyapunov candidate function is chosen,

$$V_{1,2} = \frac{1}{2}S_1^2 + \frac{1}{2}S_2^2. \tag{12}$$

The Lyapunov candidate function $V_{1,2}$ is defined as a positive definite function of the sliding surfaces S_1 and S_2. To guarantee that S_1 and S_2 converge to 0, shows asymptotic stability, the differential with respect to time of V must be negative definite. By applying the differentiation of $V_{1,2}$ with respect to time,

$$\dot{V_{1,2}} = S_1\dot{S}_1 + S_2\dot{S}_2. \tag{13}$$

Substituting the values of $\dot{S}_1$ and $\dot{S}_2$, we get

$$\begin{aligned}\dot{V_{1,2}} = S_1 \left[a_1 \left(\beta_1 x_1 x_3 + (1-u_1)\beta_2 x_1 x_2 + r_i x_2\Big(1 - \frac{x_1+x_2}{T_{\max}}\Big) - \delta x_2 - \rho x_2\right) - a_1\dot{x_{2_{ref}}} + a_2 e_1\right] \\ + S_2\left[a_3\left((1-u_2)p x_3 - c x_3 - q x_3 x_4\right) - a_3\dot{x_{3_{ref}}} + a_4 e_3\right].\end{aligned} \tag{14}$$

By substiuting the values of u_1 and u_2,

$$\begin{aligned}\dot{V_{1,2}} &= -K_1|S_1|^{\alpha+1} - K_2|S_2|^{\alpha+1}, \\ \dot{V_{1,2}} &\leq 0.\end{aligned} \tag{15}$$

Thus, the application of Lyapunov theory demonstrates the stability of the system.

3.2 Double integral sliding mode controller

DISMC is an advanced sliding mode control, incorporating an additional integral term in the formulation of the sliding surface [14]. This approach enhances system performance by improving disturbance rejection, minimizing steady-state error, and more effectively managing fluctuating dynamics in comparison to traditional SMC or Integral SMC. Consider the following sliding surfaces,

$$\begin{aligned}S_3 &= a_5 e_1 + a_6 e_2 + a_7 e_5, \\ S_4 &= a_8 e_3 + a_9 e_4 + a_{10} e_6.\end{aligned} \tag{16}$$

The coefficients of the sliding surfaces are a_5, a_6, a_7, a_8, a_9 and a_{10}. e_2 represents the integral error of e_1, e_5 is the double integral of e_1. The variable e_3 represents the error between the actual virion levels and their desired reference values. e_4 is the integral of e_3 and e_6 is the double integral of e_3. The errors can be written as,

$$\begin{aligned}e_1 &= x_2 - x_{2_{ref}}, \\ e_2 &= \int (x_2 - x_{2_{ref}})\, dt, \\ e_5 &= \int\int (x_2 - x_{2_{ref}})\, dt\, dt.\end{aligned} \tag{17}$$

Now, the derivative of the sliding surface $S_{3,4}$ with respect to time is computed to determine the input of control for virions and infected hepatocytes. By determining the input for the control u_1, we obtain:

$$u_1 = \frac{1}{a_5\beta_2 x_1 x_2}\left[a_5\beta_1 x_1 x_3 + a_5\beta_2 x_1 x_2 + K|S_3|^{\alpha} sign\left(\frac{S_3}{\phi_3}\right) + a_5 r_I x_2\left(1 - \frac{x_1+x_2}{T_{\max}}\right) - a_5\delta x_2 - a_5\rho x_2 + a_5\dot{x_{2ref}} + a_6 e_1 + a_7 e_2\right]. \tag{18}$$

To determine the control input $u_2(t)$ required for blocking and dropping virions in the HCV system, it will be

$$u_2(t) = \frac{1}{a_8 p x_2}\left[a_8 p x_2 + K_4|S_4|^{\alpha} sign\left(\frac{S_4}{\phi_4}\right) - a_8 c x_3 - a_8 q x_3 x_4 - a_8\dot{x_{3ref}} + a_9 e_3 + a_{10} e_4\right]. \tag{19}$$

To demonstrate the stability of the proposed controller, the following Lyapunov candidate function is selected,

$$V_{3,4} = \frac{1}{2}S_3^2 + \frac{1}{2}S_4^2. \tag{20}$$

The Lyapunov candidate function $V_{3,4}$ is defined as a function of positive definite for the sliding surfaces S_3 and S_4,

$$\dot{V_{3,4}} = S_3\dot{S_3} + S_4\dot{S_4}. \tag{21}$$

Substituting the values of $\dot{S_3}$ and $\dot{S_4}$, we get

$$\dot{V_{3,4}} = S_3\left[a_5\left(\beta_1 x_1 x_3 + (1-u_1)\beta_2 x_1 x_2 + r_i x_2\left(1 - \frac{x_1+x_2}{T_{\max}}\right) - \delta x_2 - \rho x_2\right) + a_5\dot{x_{2ref}} + a_6 e_1 + a_7 e_2\right] + S_4\left[a_3\left((1-u_2)p x_2 - c x_3 - q x_3 x_4\right) - a_8\dot{x_{3ref}} + a_9 e_3 + a_{10} e_4\right]. \tag{22}$$

By substiuting the values of u_1 and u_2, it becomes,

$$\begin{aligned} \dot{V_{3,4}} &= -K_3|S_3|^{\alpha_3+1} - K_4|S_4|^{\alpha_4+1}, \\ \dot{V_{3,4}} &\leq 0. \end{aligned} \tag{23}$$

Thus, the application of Lyapunov theory demonstrates the stability of the system.

3.3 Integral terminal sliding mode controller

ITSMC is an enhanced variant of sliding mode control that combines integral and terminal sliding mode techniques. The major objective is to improve the rate of covergence for the system states while preserving robustness and accuracy. ITSMC has been particularly efficient of managing nonlinear systems with disturbances and ensuring finite-time stability. Define the sliding surface of ITSMC as follows,

$$S_5 = e_1 + k_5\left[\int_0^t e_1 dt\right]^{\lambda_5}. \tag{24}$$

Here, k_5 is the design parameter associated of the sliding manifold, and λ_5 is a value satisfying the condition $1 < \lambda_5 < 2$ which is positive. The variable e_1 represents the error which tracks in the number of infected hepatocytes. By taking the derivative with respect to time for the sliding surface and determining the input of control u_1, we obtain

$$\begin{aligned} u_1 = \frac{1}{\beta_2 x_1 x_2} \Bigg[& \beta_1 x_1 x_3 + \beta_2 x_1 x_2 + K_5 |S_5|^{\alpha} sign\left(\frac{S_5}{\phi_5}\right) + r_I x_2 \left(1 - \frac{x_1 + x_2}{T_{\max}}\right) \\ & - \delta x_2 - \rho x_2 - \dot{x_{2ref}} + k_5 \lambda_5 e_1 \left[\int_0^1 e_1 dt\right]^{\lambda_5 - 1} \Bigg]. \end{aligned} \tag{25}$$

Similarly, defining the sliding surface of state variable x_3 is

$$S_6 = e_2 + k_6 \left[\int_0^t e_2 dt\right]^{\lambda_6}, \tag{26}$$

where e_2 is the error that tracks difference of virions and reference value. Determining the derivative for the sliding surfaces and computing the control input u_2, we get

$$u_2 = \frac{1}{p x_2} \left[p x_2 + K_6 |S_6|^{\alpha} sign\left(\frac{S_6}{\phi_6}\right) - c x_3 - q x_3 x_4 - \dot{x_{3ref}} + k_6 \lambda_6 e_2 \left[\int_0^1 e_2 dt\right]^{\lambda_6 - 1} \right]. \tag{27}$$

To demonstrate the stability of the proposed controller, the following Lyapunov candidate function is selected

$$V_{5,6} = \frac{1}{2} S_5^2 + \frac{1}{2} S_6^2. \tag{28}$$

The Lyapunov candidate function $V_{5,6}$ is defined as a function of positive definite for the sliding surfaces S_5 and S_6,

$$\dot{V_{5,6}} = S_5 \dot{S_5} + S_6 \dot{S_6}. \tag{29}$$

Substituting the values of $\dot{S_5}$ and $\dot{S_6}$, we get

$$\begin{aligned} & \dot{V_{5,6}} = -S_5 \left(K_5 |S_5|^{\alpha} sign\left(\frac{S_5}{\phi_5}\right)\right) - S_6 \left(K_6 |S_6|^{\alpha} sign\left(\frac{S_6}{\phi_6}\right)\right), \\ & \dot{V_{5,6}} \leq 0. \end{aligned} \tag{30}$$

Thus, the application of Lyapunov theory demonstrates the stability of the system.

3.4 Fractional order terminal sliding mode controller

FOTSMC is an advanced technique that merges sliding mode control SMC with principles from fractional calculus. This approach enhances performance in terms of convergence speed, accuracy, and robustness, especially when applied to nonlinear and uncertain systems. This method involves designing a sliding surface that combines the characteristics of fractional-order control with those of Terminal sliding mode controller (TSMC). A key advantage for FOTSMC, particularly when utilizing a terminal sliding surface with fractional order derivatives, is its ability to avoid singularity issues and achieve fast convergence which is compared to traditional Integral Terminal Sliding Mode Control. FOTSMC laws are designed to conform that the states of the

HCV system reach their reference values within a finite time, with Lyapunov's stability theory serving as the following. The sliding surface of FOTSMC is proposed and given by,

$$S_7 = c_5 D^{-\alpha} e_1 + c_6 D^{\alpha} |e_1|^{\gamma} sgn(e_1), \tag{31}$$

where c_5, c_6 and γ are positive numbers. The variable e_1 represents the error between the infected cells and their reference values, defined as $e_1 = x_2 - x_{2_{ref}}$. D is fractional operator and defined as,

$${}_a\mathbb{D}_t^{\alpha} = \begin{cases} \dfrac{d^{\alpha}}{dt^{\alpha}}, & \mathbb{R}(\alpha) > 0, \\ 1, & \mathbb{R}(\alpha) = 0, \\ \displaystyle\int_{\alpha}^{t} (d\tau)^{-\alpha}, & \mathbb{R}(\alpha) < 0, \end{cases} \tag{32}$$

where α represent fractional operator order and $\mathbb{R}(\alpha)$ is real set number [1]. When integer-order controllers attains its objectives, fractional-order controllers enhance realism by modeling memory and hereditary traits in biological systems. This results in smoother control actions and better convergence. Among all, the FOTSMC showed superior regulation with lower control effort, making it a promising tool for designing optimized treatment strategies. The operator of fractional order which is defined in various ways, including several different definitions.

Definition 3.1. [13] *Reimann-Liouville fractional integral with the derivative of αth order for the function $f(t)$ w.r.t time is*

$$\begin{aligned} {}_a\mathbb{D}_t^{\alpha} &= \frac{d^{\alpha}}{dt^{\alpha}} f(t) = \frac{1}{\Gamma(m-\alpha)} \frac{d^m}{dt^m} \int_{\alpha}^{t} \frac{f(\tau)}{(t-\tau)^{\alpha-m+1}} d\tau, \\ {}_a\mathbb{D}_t^{-\alpha} &= I^{\alpha} f(t) = \frac{1}{\Gamma(\alpha)} \int_{\alpha}^{t} \frac{f(\tau)}{(t-\tau)^{1-\alpha}} d\tau. \end{aligned} \tag{33}$$

Here, $t - \alpha$ is interval integration and "m" is a positive integer which is larger than "a" such as $m - 1 < \alpha < m$.

Definition 3.2. [13] *The Caputo derivative of fractional-order α for the function $f(t)$ is defined as,*

$${}_a\mathbb{D}_t^{\alpha} f(t) = \begin{cases} \dfrac{1}{\Gamma(\nu-\alpha)} \displaystyle\int_{\alpha}^{t} \frac{f^{\nu}(\tau)}{(t-\tau)^{\alpha} - \nu + 1} d\tau, & (\nu - 1 \leq \alpha < \nu), \\ \dfrac{d^m}{dt^m} f(t), & (\alpha = \nu). \end{cases} \tag{34}$$

Definition 3.3. [1] *Order α GL definition is defined as,*

$$\alpha^{GL}\mathbb{D}_t^{\alpha} f(t) = \lim_{ts \to 0} \frac{1}{ts^{\alpha}} \sum_{j=0}^{\frac{(t-\alpha)}{h}} (-1)^j \binom{\alpha}{j} f(t - jh), \tag{35}$$

$$\binom{\alpha}{j} = \frac{\Gamma(\alpha+1)}{\Gamma(j+1)\Gamma(\alpha-j+1)}, \tag{36}$$

where the gamma function is denoted by $\Gamma(.)$ and time step by ts.

Taking derivative of the sliding surface S_7, we get

$$\dot{S}_7 = c_5 D^{1-\alpha} e_1 + c_6 \gamma D^{\alpha} |e_1|^{\gamma-1} \dot{e}_1. \tag{37}$$

By applying $D^{-\alpha}$ on both sides of (37), we get

$$D^{1-\alpha}\dot{S}_7 = c_5 D^{1-2\alpha} e_1 + c_6\gamma|e_1|^{\gamma-1}\dot{e_1}. \tag{38}$$

The term $D^{1-\alpha}$ denotes the fractional derivative term. We can represent our notation as $D^{\hat{\alpha}}$ for our simplicity. A more simplified form of (38) can be expressed as,

$$D^{\hat{\alpha}}\dot{S}_7 = c_5 D^{1-2\alpha} e_1 + c_6\gamma|e_1|^{\gamma-1}\dot{e_1}. \tag{39}$$

Taking derivative for e_1, we get

$$\dot{e_1} = \frac{dx_2}{dt} - \dot{x_{2ref}}. \tag{40}$$

Substituting (40) into the (39), gives

$$D^{\hat{\alpha}}\dot{S}_7 = c_5 D^{1-2\alpha} e_1 + c_6\gamma|e_1|^{\gamma-1}\Big(\beta_1 x_1 x_3 + (1-u_1)\beta_2 x_1 x_2 + r_I x_2\left(1 - \frac{x_1+x_2}{T_{\max}}\right) - \delta x_2 - \rho x_2 - \dot{x_{2ref}}\Big).$$

By solving the above equation for the control input $u_1(t)$, we get

$$\begin{aligned} u_1 &= u_{nom} + u_{sw}, \\ u_{nom} &= \frac{1}{\beta_2 x_1 x_2}\left[\beta_1 x_1 x_3 + \beta_2 x_1 x_2 - \frac{c_5 D^{1-2\alpha} e_1 |e_1|^{1-\gamma}}{c_6\gamma} + r_I x_2\left(1 - \frac{x_1+x_2}{T_{\max}}\right) - \delta x_2 - \rho x_2 - \dot{x_{2ref}}\right], \\ u_{sw} &= \frac{1}{\beta_2 x_1 x_2}\left[-\frac{K_{r_3}}{\gamma c_6} sgn(S_7)|e_1|^{1-\gamma}\right]. \end{aligned} \tag{41}$$

Similarly, the sliding surface for the state variable (x_3) is defined as,

$$S_8 = c_7 D^{-\alpha} e_2 + c_8 D^{\alpha}|e_2|^{\gamma} sgn(e_2), \tag{42}$$

where c_7 and c_8 are positive numbers. The variable e_2 represents the error between the virion levels and their reference values, defined as $e_2 = x_3 - x_{3_{ref}}$. Derivating the sliding surface S_8 and substituting the values of $\dot{e_2}$, then,

$$D^{\hat{\alpha}}\dot{S}_8 = c_7 D^{1-2\alpha} e_2 + c_8\gamma|e_2|^{\gamma-1}\Big((1-u_2)pI - cV - qVW - \dot{x_{3ref}}\Big). \tag{43}$$

Solving (43) for the control input $u_2(t)$, then,

$$\begin{aligned} u_2 &= u_{nom} + u_{sw}, \\ u_{nom} &= \frac{1}{px_2}\left[px_2 - \frac{c_7 D^{1-2\alpha} e_2 |e_2|^{1-\gamma}}{c_8\gamma} - cx_3 - qx_3 x_4 - \dot{x_{3ref}}\right], \\ u_{sw} &= \frac{1}{px_2}\left[-\frac{K_{r_4}}{\gamma c_8} sgn(S_7)|e_2|^{1-\gamma}\right]. \end{aligned} \tag{44}$$

The stability of the closed-loop system for the proposed control paradigm is guaranteed by applying the Lyapunov stability theorem, utilizing the selection of $V_i = \frac{1}{2}S_i^2$. The application of a

fractional operator $D^{\hat{\alpha}}$ to the Lyapunov function V_i yields the subsequent expression,

$$D^{\hat{\alpha}}V_1 \leq S_i D^{\hat{\alpha}} S_i + \sum_{j=1}^{\infty} \frac{\tau(1+\bar{\alpha})}{\tau(1+\bar{\alpha}-j)(1+j)} D^j S_i D^{\bar{\alpha}-j} S_i. \tag{45}$$

Consider the following inequality,

$$\sum_{j=1}^{\infty} \frac{\tau(1+\bar{\alpha})}{\tau(1+\bar{\alpha}-j)(1+j)} D^j S_i D^{\bar{\alpha}-j} S_i \leq \rho |S_i|. \tag{46}$$

Furthermore,

$$\begin{aligned}
&D^{\hat{\alpha}}V_1 \leq S_i D^{\hat{\alpha}} S_i + \lambda_3 S_i,\\
&D^{\hat{\alpha}}V_1 \leq c_5 D^{1-2\alpha} e_1 + c_6 \gamma |e_1|^{\gamma-1}\\
&\qquad \times \left(\beta_1 x_1 x_3 + (1-u_1)\beta_2 x_1 x_2 + r_I x_2 \left(1 - \frac{x_1+x_2}{T_{\max}}\right) - \delta x_2 - \rho x_2 - \dot{x_{2_{ref}}}\right) + \lambda_3 S_7,\\
&D^{\hat{\alpha}}V_2 \leq c_7 D^{1-2\alpha} e_2 + c_8 \gamma |e_2|^{\gamma-1} \Big((1-u_2)pI - cV - qVW - \dot{x_{3_{ref}}}\Big) + \lambda_3 S_8.
\end{aligned} \tag{47}$$

Finally, by simplification we get the following,

$$D^{\hat{\alpha}}V_i \leq -\lambda_i |S_i| + \rho |S_i|. \tag{48}$$

By choosing λ_i, such that $\lambda_i |S_i| > \rho |S_i|$, $D^{\hat{\alpha}}V_i$ is always negative.

Theorem 3.1. *By applying the Lyapunov stability theorem, by considering the fractional-order sliding surfaces $S_{7,8}$, which ensure that the fractional-order sliding surface remains stable and asymptotically approaches zero.*

Proof. Let us consider $S_7 + S_8$ such that,

$$S_7 + S_8 = \Big[c_5 D^{-\alpha} e_1 + c_6 D^{\alpha} |e_1|^{\gamma} sgn(e_1) + c_7 D^{-\alpha} e_2 + c_8 D^{\alpha} |e_2|^{\gamma} sgn(e_2)\Big]. \tag{49}$$

Consider the fractional dynamics error as,

$${}_a\mathbb{D}_t^{\alpha} e_1 + {}_a\mathbb{D}_t^{\alpha} e_2 = -\lambda_1 e_1 - \lambda_2 e_2, \qquad 0 < \alpha < 1. \tag{50}$$

Considering a Lyapunov function associated with the error variables (e_1, e_2), it is constructed as follows,

$$V_{e_1,e_2} = \frac{1}{2} e_1^2 + \frac{1}{2} e_2^2. \tag{51}$$

Taking fractional derivative on both sides,

$$\begin{aligned}
{}_a\mathbb{D}_t^{\alpha} V_{e_1,e_2} &= \frac{1}{2} {}_a\mathbb{D}_t^{\alpha} e_1^2 + \frac{1}{2} {}_a\mathbb{D}_t^{\alpha} e_2^2,\\
&\leq e_1 {}_a\mathbb{D}_t^{\alpha} e_1 + e_2 {}_a\mathbb{D}_t^{\alpha} e_2 = -\lambda_1 e_1^2 - \lambda_2 e_2^2.
\end{aligned} \tag{52}$$

The stability of the surfaces was proved. □

Remark 3.1. *The Caputo derivative is well-suited for systems where the fractional order captures memory effects, and it integrates smoothly with Lyapunov-based stability analysis and control design. The fractional derivative $\alpha \in (0, 1]$ is defined in the Caputo sense, incorporating a convolution integral with a power-law memory kernel to effectively capture memory effects in dynamical systems. The decay rate of this memory kernel, which acts as a time-correlation function, is governed by the value of α. Specifically, smaller values of α correspond to slower decay, indicating stronger memory (long-term dependence). As α approaches 1, the memory effect diminishes.*

Remark 3.2. *The Lyapunov-based stability analysis is widely used in control theory, the novelty of this work lies in constructing customized Lyapunov functions specific to each nonlinear control scheme, including fractional-order dynamics. These functions are carefully designed to match the structure of the sliding surfaces and control objectives, enabling more precise stability analysis. In particular, the fractional-order Lyapunov function accounts for memory effects, which are often neglected in classical integer-order approaches. This enhances the biological realism and analytical depth of the proposed stability proofs.*

4 Numerical Simulations

In this section, we assesses the effectiveness of the suggested control input laws: ISMC (10) and (11), DISMC (18) and (19), ITSMC (25) and (27), and FOTSMC (41) and (44). The evaluation is provided through simulation results conducted over a period of 50 days. The following are the initial values: uninfected hepatocytes at 555 IU/L, infected hepatocytes at $50,000$ IU/L, virions at $20,000$ IU/L, and antibodies at $2,000$ IU/L. These values are calculated by Polymerase Chain Reaction(PCR). To achieve the desired equilibrium point represented by $x = [1840690, 0, 0, 289213]^T$, control measures were implemented to regulate the levels of uninfected and infected hepatocytes, virions and antibodies.

The initial state of the error dynamics substantially affects the duration needed for the system state to reach the intended reference value. While choosing a high initial value for the reachability time of the double integrals can reduce convergence time, it leads to initiating the process of chemotherapy with the injection of high-dose, is undesirable. In this proposed control approach, the chemotherapy dosage is gradually initiated by establishing the initial state for the dynamics of error to 0. For each proposed controller, the initial state for the error dynamics is set as $e_i = 0$. The defined reference values for infected hepatocytes, virions and uninfected are defined as $x_{2_{ref}} = 0$, $x_{3_{ref}} = 0$, and $T_{\max} = 800000$, respectively. The proposed controllers for the design parameters are determined using a method of trial and error. The target reference value is achieved by modifying the gain value. The values and parameters of the nonlinear HCV system are provided as follows;

- $s = 2400000, \quad \beta_1 = 0.0000001, \quad \beta_2 = 0.000001, \quad c = 10, \quad p = 20.$
- $g = 0.0005, \quad q = 0.0001, \quad r_T = 1, \quad r_i = 0.7, \quad d_T = 0.003, \quad \delta = 0.002.$

For the ISMC, the values for the gains parameters are defined as follows;

- $a_1 = 9780, \quad a_2 = 4, \quad a_3 = 1, \quad a_4 = 1.$
- $K_1 = 6300, \quad K_2 = 35000, \quad \alpha = 0.5, \quad \phi_1 = \phi_2 = 0.5.$

For the DISMC, the values for the gains parameters are defined as follows;

- $a_5 = 9000, \quad a_6 = 1, \quad a_7 = 12,590,000, \quad a_8 = 7500, a_9 = 1, \quad a_{10} = 90000.$

- $K_3 = 65,000, \quad K_4 = 65,000, \quad \alpha = 0.5, \quad \phi_3 = \phi_4 = 0.5.$

For the ITSMC, the values for the gains parameters are defined as follows;

- $\lambda_5 = 1.5, \quad \lambda_6 = 1.5.$
- $k_5 = 6500, \quad k_6 = 90,000, \quad \alpha = 0.5, \quad \phi_5 = \phi_6 = 0.5.$

For the FOTSMC, the values for the gains parameters are defined as follows;

- $c_5 = 0.15, \quad c_6 = 0.01, \quad c_7 = 0.20, \quad c_8 = 0.0010.$
- $k_{r_3} = 0.050, \quad k_{r_4} = 0.0001, \quad \gamma = 1.5, \quad \alpha = 0.5, \quad \phi_3 = \phi_4 = 0.5.$

Here, the system behavior of model (2) without control (i.e., without drug administration) is illustrated in Figure 3. This uncontrolled behavior demonstrates the natural tendencies and responses of the system without any external influences. Without any drug usage, the number of virions and infected individuals is high, while the number of uninfected individuals is decreasing. This work utilizes FOTSMC, ITSMC, DISMC, and ISMC to effectively track the reduction of virion concentration and infected hepatocytes to their reference values. The goal is to minimize liver toxicity and maintain optimal liver function while achieving effective antiviral activity. By combining these different approaches, this work aims to find the most efficient and safe method for treating HCV without causing significant damage to healthy liver cells. Through careful monitoring and adjustment of dosages, but it may strike a balance between efficacy and safety in their treatment approach.

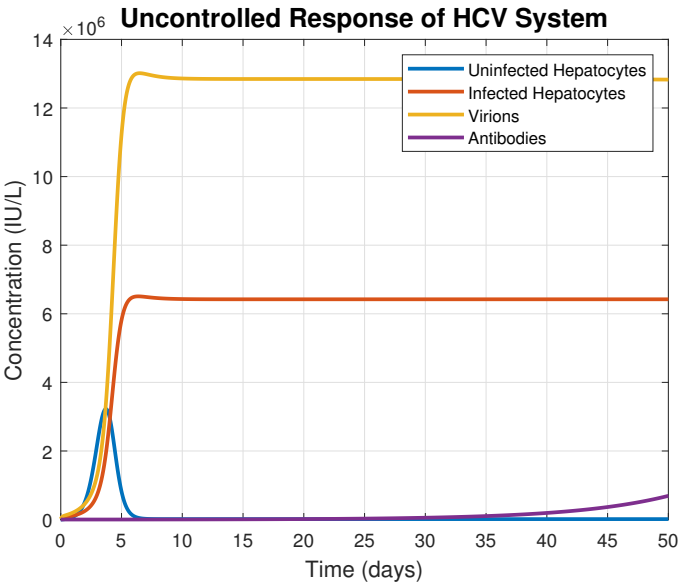

Figure 3: Behavior of model (3) without any controls.

After exposure to the virus, the drug efficacy u_1 remained at its highest level for an extended period because the virus did not diminish quickly. Similarly, the drug efficacy u_2 also stayed at its highest level for a longer duration as the virus began to decrease. To ensure the drug quantity

remains within safe parameters, the upper limits for drug efficacy u_1 and u_2 are established at 0.96. The control inputs of u_1 and u_2 for ISMC, DISMC and FOTSMC is shown in the Figures 4, 5 and 6. By comparing all these FOTSMC shows the less usage of drug and faster lowering rate of disease.

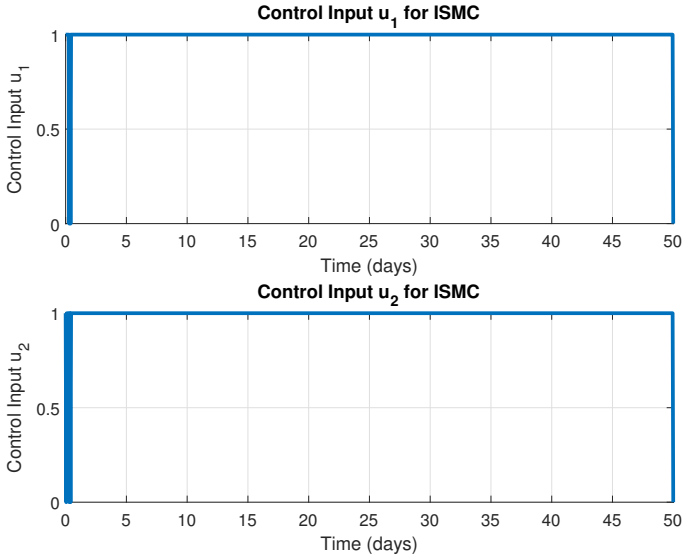

Figure 4: Control input of ISMC in HCV.

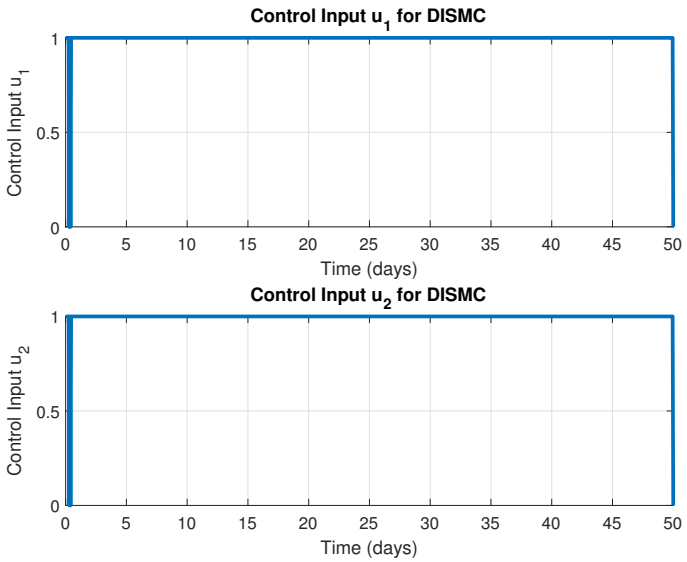

Figure 5: Control input of DISMC in HCV.

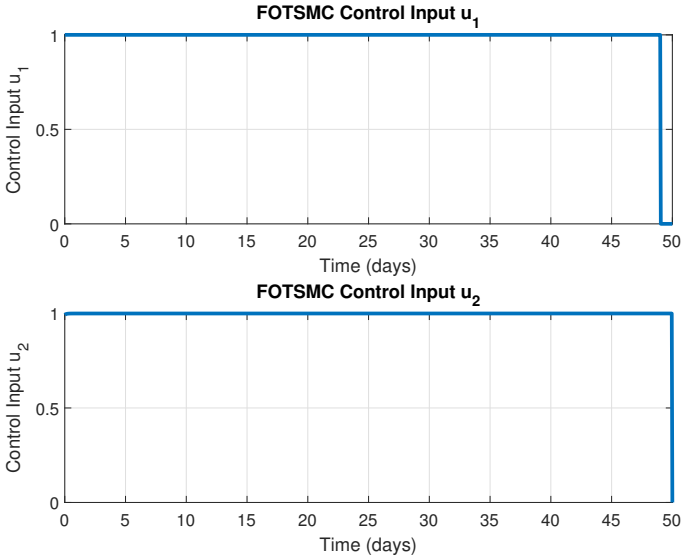

Figure 6: Control input of FOTSMC in HCV.

Here, we divide into four distinct subsections. The first subsection describes the reactions of uninfected individuals to the injection of drug using the proposed controllers. In a similar manner, the subsequent subsections detail the characteristics of infected individuals, virions, and antibodies, respectively. The final subsection concludes with a comparison of all proposed controllers, focusing on treatment response, SSE and chattering their performance in control and reduction of HCV.

4.1 Uninfected hepatocytes responses

The behavior of uninfected hepatocytes in response to HCV infection, together with the evaluation of all designed controllers, has been thoroughly investigated. Figure 7 illustrates the response of uninfected hepatocytes following the administration of the drug. A significant rise in the population of uninfected hepatocytes is observed, nearing $T_{\max}$, which denotes the peak concentration of these cells within the liver. Time for uninfected hepatocytes to reach equilibrium is comparable for both ISMC and FOTSMC until it attains its peak. Uninfected hepatocytes demonstrated steady-state error with ISMC, while FOTSMC showed a reduced steady-state error. Furthermore, FOTSMC exhibited reduced SSE in comparison to DISMC. ITSMC demonstrated remarkable tracking of uninfected hepatocytes to $T_{\max}$, achieving improved transient time and reduced SSE overall.

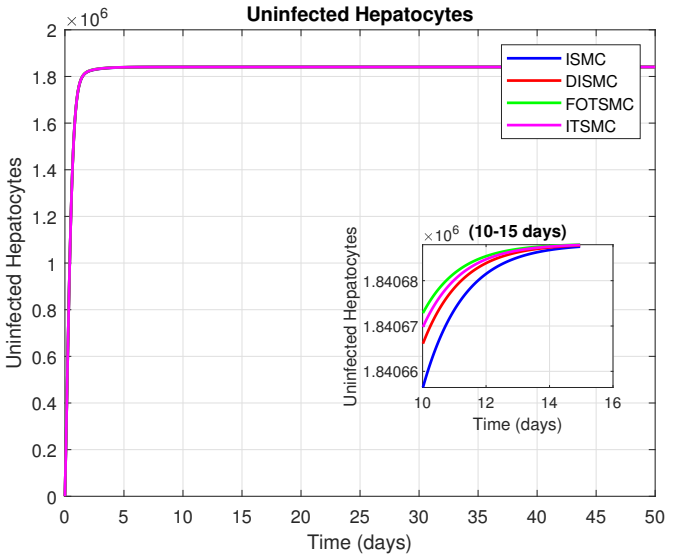

Figure 7: Comparision of different SMC in uninfected hepatocytes.

4.2 Infected hepatocytes responses

Figure 8 illustrates the dynamics of infected hepatocytes in response to the proposed controllers. The results indicate that the tracking time to reference values is significantly quicker with FOTSMC in comparison to ISMC, DISMC, and ITSMC. However, ISMC exhibits a significant SSE in its ability to track the reference value. In comparison, hepatocytes that are infected with FOTSMC attain the reference value in roughly $12 - 14$ days without any SSE. Overall, FOTSMC demonstrates reduced SSE and a faster response to achieve the reference value in infected hepatocytes when compared to other sliding mode controllers.

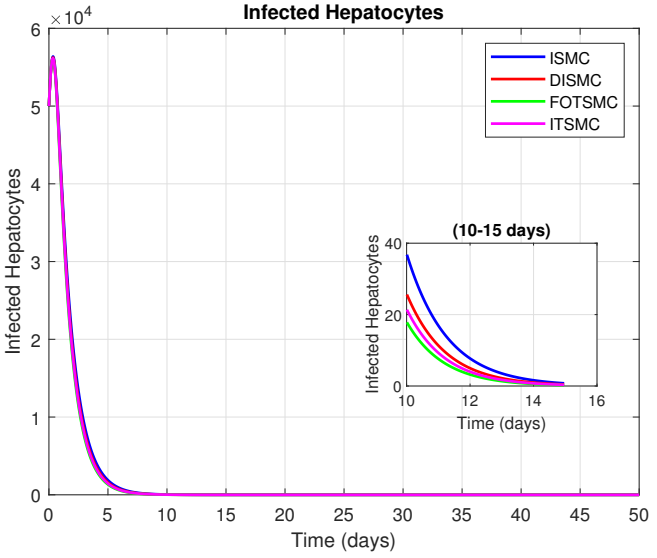

Figure 8: Comparision of different SMC in infected hepatocytes.

4.3 Virions responses

Figure 9 shows the behavior of the virions. The FOTSMC method enables a rapid convergence to the reference value, whereas the ISMC method leads to a significant SSE throughout the tracking process. The duration for tracking virions with FOTSMC spans from 12 to 14 days after administration of Ribavirin and Peg-IFN-α. In this, compared to other sliding mode controllers FOTSMC reaches its reference values soon that which represents in decreasing the virions so quickly.

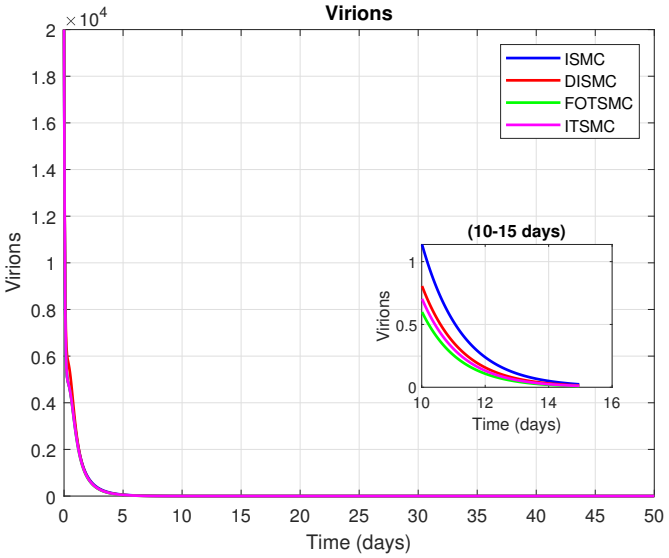

Figure 9: Comparision of different SMC in virions compartment.

4.4 Antibodies responses and discussion

Figure 10 illustrates the response of the antibodies to the proposed controllers showing a higher rate with DISMC compared to FOTSMC. In the Antibodies, FOTSMC exhibited a lower performance relative to other sliding mode controllers. A comparison has been made among the performances of FOTSMC, DITSMC, ITSMC and ISMC. The proposed controllers are evaluated based on their characteristics, including settling time, SSE, chattering during convergence to the reference level, as well as the stabilization period. Uninfected hepatocytes reach convergence at the designated point within 5 days. The duration for settling is approximately 10 days without any SSE involved. The tracking of virions and hepatocytes which are infected to their reference levels, with reduced SSE, is achieved within 10 days utilizing FOTSMC. FOTSMC assesses the performance of alternative controllers based on transient response, overshoot, SSE and settling times. It demonstrates exceptional efficacy in diminishing and monitoring virions and infected hepatocytes.

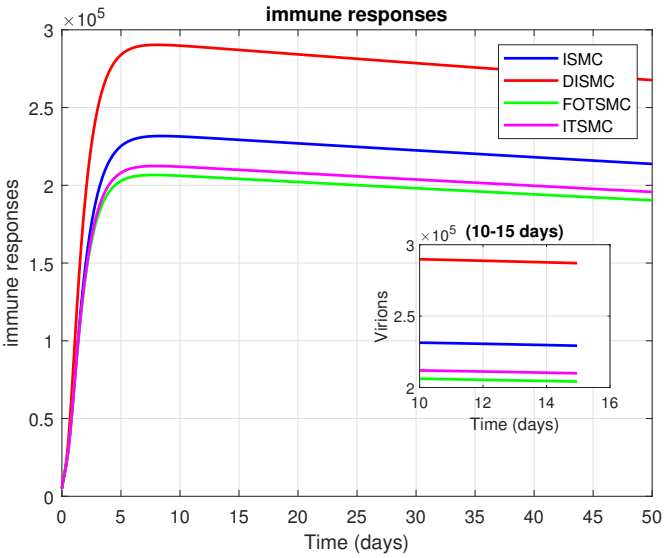

Figure 10: Comparision of different SMC in immune responses.

5 Conclusions

This work examined the dynamics of dual transmission of HCV model with control inputs. A combined dose of interferon and ribavirin is used as a control strategy to suppress infected hepatocytes and virions. This study relies on dynamic nonlinear controllers such as those for FOTSMC, DISMC, ITSMC, and ISMC. Control input laws are being developed to reduce and block the quantity of hepatocytes of infected and virions to targeted levels, while adhering to the constraints of treatment efficacy. The simulation results demonstrate that the concentrations of virions and infected hepatocytes can attain their reference values respectively within 12 to 14 days. Furthermore, the simultaneous injection of the antiviral agent peg-IFN-α and ribavirin results in a more rapid reduction of both virions and infected hepatocytes. By incorporating the integral, the SSE has been reduced, as observed in the DISMC. FOTSMC have less SSE and it was found better comparing the other sliding mode controllers. This comparative study highlights the feasibility of these controllers, with the fractional-order terminal sliding mode controller demonstrating superior performance in the overall elimination of virions and infected hepatocytes. In future studies, we plan to apply integral super twisting sliding mode control and adaptive sliding mode control.

Acknowledgement The authors are grateful to anonymous referees for their remarks and suggestions that helped improve the manuscript.

Conflicts of Interest The authors declare that there is no conflict of interests regarding the publication of this article.

References

[1] M. P. Aghababa (2014). A Lyapunov-based control scheme for robust stabilization of fractional chaotic systems. *Nonlinear Dynamics*, *78*(3), 2129–2140. https://doi.org/10.1007/s11071-014-1594-8.

[2] O. P. Agrawal, O. Defterli & D. Baleanu (2010). Fractional optimal control problems with several state and control variables. *Journal of Vibration and Control*, *16*(13), 1967–1976. https://doi.org/10.1177/1077546309353361.

[3] M. Farman, C. Xu, P. Abbas, A. Sambas, F. Sultan & K. S. Nisar (2025). Stability and chemical modeling of quantifying disparities in atmospheric analysis with sustainable fractal fractional approach. *Communications in Nonlinear Science and Numerical Simulation*, *142*, Article ID: 108525. https://doi.org/10.1016/j.cnsns.2024.108525.

[4] M. S. D. Haggar & J. M. Ntaganda (2023). Perturbation iteration method compared with direct method and fuzzy logic strategy for solving an optimal control problem of an uninfected hepatitis B virus dynamics. *Malaysian Journal of Mathematical Sciences*, *17*(3), 227–239. https://doi.org/10.47836/mjms.17.3.01.

[5] M. S. D. Haggar & J. M. Ntaganda (2025). Efficacy of the perturbation iteration method in testing the response of hepatitis C virus treatment on the dynamics of uninfected and infected hepatocytes. *Universal Journal of Mathematics and Mathematical Sciences*, *21*(1), 13–37. https://doi.org/10.17654/2277141725002.

[6] A. Hamza, M. Uneeb, I. Ahmad, K. Saleem & Z. Ali (2024). Variable structure based control strategy for treatment of HCV infection. *Biomedical Signal Processing and Control*, *89*, Article ID: 105803. https://doi.org/10.1016/j.bspc.2023.105803.

[7] H. K. Khalil & J. W. Grizzle (2002). *Nonlinear Systems* volume 3. Prentice Hall, Upper Saddle River, New Jersey.

[8] K. S. Kim, S. Kim & I. H. Jung (2018). Hopf bifurcation analysis and optimal control of treatment in a delayed oncolytic virus dynamics. *Mathematics and Computers in Simulation*, *149*, 1–16. https://doi.org/10.1016/j.matcom.2018.01.003.

[9] C. Maharajan, C. Sowmiya & C. Xu (2024). Delay dependent complex-valued bidirectional associative memory neural networks with stochastic and impulsive effects: An exponential stability approach. *Kybernetika*, *60*(3), 317–356. http://doi.org/10.14736/kyb-2024-3-0317.

[10] S. Majee, S. Barman, A. Khatua, T. K. Kar & S. Jana (2023). The impact of media awareness on a fractional-order SEIR epidemic model with optimal treatment and vaccination. *The European Physical Journal Special Topics*, *232*(14), 2459–2483. https://doi.org/10.1140/epjs/s11734-023-00910-9.

[11] J. Mondal, P. Samui, A. N. Chatterjee & B. Ahmad (2024). Modeling hepatocyte apoptosis in chronic HCV infection with impulsive drug control. *Applied Mathematical Modelling*, *136*, Article ID: 115625. https://doi.org/10.1016/j.apm.2024.07.032.

[12] A. U. Neumann, N. P. Lam, H. Dahari, D. R. Gretch, T. E. Wiley, T. J. Layden & A. S. Perelson (1998). Hepatitis C viral dynamics in vivo and the antiviral efficacy of interferon-α therapy. *Science*, *282*(5386), 103–107. https://doi.org/10.1126/science.282.5386.103.

[13] I. Podlubny (1998). *Fractional Differential Equations: An Introduction to Fractional Derivatives, Fractional Differential Equations, to Methods of their Solution and some of their Applications* volume 198. Academic Press, San Diego, California.

[14] R. Pradhan & B. Subudhi (2015). Double integral sliding mode MPPT control of a photovoltaic system. *IEEE Transactions on Control Systems Technology*, *24*(1), 285–292. https://doi.org/10.1109/TCST.2015.2420674.

[15] A. Rehman, R. Ghias, S. H. Ahmed, S. Saleem, I. Ahmad & H. I. Sherazi (2024). Enhancing antiviral therapies through nonlinear control of Hepatitis C virus dynamics. *Biomedical Signal Processing and Control*, *97*, Article ID: 106727. https://doi.org/10.1016/j.bspc.2024.106727.

[16] F. A. Rihan, A. A. Arafa, R. Rakkiyappan, R. Chinnathambi & Y. Xu (2021). Fractional-order delay differential equations for the dynamics of hepatitis C virus infection with IFN-α treatment. *Alexandria Engineering Journal*, *60*(5), 4761–4774. https://doi.org/10.1016/j.aej.2021.03.057.

[17] F. A. Rihan, M. Sheek-Hussein, A. Tridane & R. Yafia (2017). Dynamics of hepatitis C virus infection: mathematical modeling and parameter estimation. *Mathematical Modelling of Natural Phenomena*, *12*(5), 33–47. https://doi.org/10.1051/mmnp/201712503.

[18] F. A. Rihan & H. J. Alsakaji (2021). Analysis of a stochastic HBV infection model with delayed immune response. *Mathematical Biosciences and Engineering*, *18*(5), 5194–5220. https://doi.org/10.3934/mbe.2021264.

[19] F. A. Rihan & R. Chinnathambi (2021). Dynamics of tumor-immune system with random noise. *Mathematics*, *9*(21), Article ID: 2707. https://doi.org/10.3390/math9212707.

[20] M. Sadki, S. Harroudi & K. Allali (2024). Local and global stability of an HCV viral dynamics model with two routes of infection and adaptive immunity. *Computer Methods in Biomechanics and Biomedical Engineering*, *27*(11), 1510–1537. https://doi.org/10.1080/10255842.2023.2245941.

[21] X. Shi, Y. Jin, X. Zhou & C. Wang (2023). Sliding mode control for fractional-order time-varying delay systems under external excitation. *Journal of Vibration and Control*, *29*(7–8), 1713–1725. https://doi.org/10.1177/10775463211069201.

[22] V. K. Shukla, M. C. Joshi, P. K. Mishra & C. Xu (2024). Adaptive fixed-time difference synchronization for different classes of chaotic dynamical systems. *Physica Scripta*, *99*(9), Article ID: 095264. https://doi.org/10.1088/1402-4896/ad6ec4.

[23] J. S. H. Simon & J. F. T. Rabago (2018). Optimal control for a predator-prey model with disease in the prey population. *Malaysian Journal of Mathematical Sciences*, *12*(2), 269–285.

[24] T. Stocks, L. J. Martin, S. Kühlmann-Berenzon & T. Britton (2020). Dynamic modeling of hepatitis C transmission among people who inject drugs. *Epidemics*, *30*, Article ID: 100378. https://doi.org/10.1016/j.epidem.2019.100378.

[25] X. Wang, X. Meng & L. Rong (2024). Global dynamics of a multiscale model for hepatitis C virus infection. *Applied Mathematics Letters*, *149*, Article ID: 108904. https://doi.org/10.1016/j.aml.2023.108904.

[26] X. Wang, H. Zhao & L. Wang (2025). Dynamics of an age-structured multiscale hepatitis C virus model with two infection modes and antibody immune response. *Mathematical Methods in the Applied Sciences*, *48*(3), 2693–2725. https://doi.org/10.1002/mma.10352.

[27] World Health Organization. Hepatitis C. Technical report World Health Organization 2025. https://www.who.int/news-room/fact-sheets/detail/hepatitis-c.

[28] S. B. Woyesa & K. D. Amente (2023). Hepatitis C virus dynamic transmission models among people who inject drugs. *Infection and Drug Resistance*, *16*, 1061–1068. https://doi.org/10.2147/IDR.S403133.

[29] C. Xu, M. Farman, Y. Pang, Z. Liu, M. Liao, L. Yao, A. Shehzad & D. Amilo (2025). Mathematical analysis and dynamical transmission of SEI_rI_sR model with different infection stages by using fractional operator. *International Journal of Biomathematics*, pp. Article ID: 2450151. https://doi.org/10.1142/S1793524524501511.

[30] C. Xu, M. Farman, A. Shehzad & K. Sooppy Nisar (2025). Modeling and Ulam–Hyers stability analysis of oleic acid epoxidation by using a fractional-order kinetic model. *Mathematical Methods in the Applied Sciences*, *48*(3), 3726–3747. https://doi.org/10.1002/mma.10510.

[31] C. Xua, M. Liaob, M. Farman & A. Shehzade (2024). Hydrogenolysis of glycerol by heterogeneous catalysis: A fractional order kinetic model with analysis. *MATCH Communications in Mathematical and in Computer Chemistry*, *91*(3), 635–664. https://doi.org/10.46793/match.91-3.635X.